Doping effects on structural and magnetic properties of Heusler alloys $Fe_2Cr_{1-x}Co_xSi$

Yifan Liu,[1,a] Lizhu Ren,[1] Yuhong Zheng,[1] Shikun He,[2] Yang Liu,[1] Ping Yang,[3] Hyunsoo Yang,[1] and Kie Leong Teo[1]

[1]*Department of Electrical and Computer Engineering, National University of Singapore, 4 Engineering Drive 3, Singapore 117583*

[2]*School of Physical and Mathematical Sciences, Nanyang Technological University, 21 Nanyang Link, Singapore 637371*

[3]*Singapore Synchrotron Light Source, National University of Singapore, 5 Research Link, Singapore 117603*

(Presented 10 November 2017; received 2 October 2017; accepted 2 January 2018; published online 19 January 2018)

In this work, 30nm $Fe_2Cr_{1-x}Co_xSi$ (FCCS) magnetic films were deposited on Cr buffered MgO (100) substrates by sputtering. $Fe_2Cr_{0.5}Co_{0.5}Si$ exhibits the largest magnetization and optimal ordered $L2_1$ cubic structure at in-situ annealing temperature (T_{ia}) of 450°C. The Co composition dependence of crystalline structures, surface morphology, defects, lattice distortions and their correlation with the magnetic properties are analyzed in detail. The Co-doped samples show in-plane *M-H* loops with magnetic squareness ratio of 1 and increasing anisotropy energy density with Co composition. Appropriate Co doping composition promotes $L2_1$ phase but higher Co composition converts $L2_1$ to $B2$ phase. Doping effect and lattice mismatch both are proved to increase the defect density. In addition, distortions of the FCCS lattice are found to be approximately linear with Co composition. The largest lattice distortion (*c/a*) is 0.969 for $Fe_2Cr_{0.25}Co_{0.75}Si$ and the smallest is 0.983 for Fe_2CrSi. Our analyses suggest that these tetragonal distortions mainly induced by an elastic stress from Cr buffer account for the large in-plane anisotropy energy. This work paves the way for further tailoring the magnetic and structural properties of quaternary Heusler alloys. https://doi.org/10.1063/1.5007289

I. INTRODUCTION

Heusler alloys are promising candidates for spintronic applications such as magnetic random access memory (MRAM) due to their low damping, high spin polarization and high Curie temperature.[1–4] Co-based Heusler alloys have been extensive investigated,[5–8] however, their large magnetizations are not favorable to reduce the switching current density in device applications. Fe-based Heusler alloys exhibit similar level of damping value and lower saturate magnetization compared with Co-based Heusler alloys.[9–11] Furthermore, Fe-based Heusler alloy is good for achieving perpendicular magnetic anisotropy (PMA). On one hand, the introduction of MgO interfaces may develop PMA through Fe-3d and O-2d hybridization. On the other hand, it has been revealed that large lattice mismatch between buffer layer and Heusler alloys can enhance PMA.[12,13] Co can be doped into Fe_2CrSi to tune the Fermi level and hence optimize its properties.[14,15] Due to difference in lattice constant (5.5Å-5.6Å, and ~5.7Å for Fe and Co based Heusler alloy, respectively), and hence lattice mismatch between film and buffer layer, the stress can also be tuned through Co doping. It has been reported that the strain induced by epitaxial misfit can change the magneto-elastic energy

[a]Electronic mail: liuyifan@u.nus.edu

and magnetic anisotropy.[16] The in-plane anisotropy could linearly change with lattice deformation.[17] The annealing temperature dependence of lattice strains and its effect on magnetic anisotropies of Co-based Heusler alloy has been studied.[18] However, the doping dependence of defect and strain in Fe-based Heusler alloy is still lacking. Besides, some defects or misfit in Heusler alloys can also affect other properties such as resistivity and spin polarization.[19,20] Thus, it's important to study strain or lattice distortion in the FCCS.

We have previously demonstrated high perpendicular and in-plane tunnel magnetoresistance ratio (TMR) by optimizing FCCS in magnetic tunnel junction (MTJ).[21,22] In this work, we provide a detailed investigation of the structural and magnetic properties of Cr buffered FCCS dependent on T_{ia} and Co doping composition. The defects and lattice distortion affected by Co doping are also discussed.

II. EXPERIMENT

All samples were deposited on crystalline MgO(100) substrates by ultra-high vacuum (UHV) magnetron sputtering system. The base pressure is lower than 10^{-8} Torr. 30nm $Fe_2Cr_{1-x}Co_xSi$ layers were deposited on 35nm Cr buffered MgO(100) by co-sputtering Fe_2CrSi and Fe_2CoSi targets. By controlling the sputtering power of individual targets, different compositions of Cr and Co were achieved. A total deposition speed of around 0.3Å/s was maintained. MgO substrates were firstly annealed at 600°C for 1 hour to degas and enhance the surface quality.[18,23] The Cr buffer layer was annealed at 700°C for 1 hour to promote a crystalline structure. Finally, the stacks were capped with 3 nm Ru layer. All the films were deposited at room temperature (RT). The first series of samples are $Fe_2Cr_{0.5}Co_{0.5}Si$ (30nm) in situ annealed at different T_{ia} (350°C~500°C) for 30 mins. The second series of samples $Fe_2Cr_{1-x}Co_xSi$ (30nm) films (x=0~1) are annealed at 450°C for 30 mins. The magnetic moment and anisotropy of the samples are investigated by vibrating sample magnetometer (VSM). The structural properties are analyzed by synchrotron light source X-ray diffraction (XRD). The surface morphology is characterized by atomic force microscopy (AFM). The defects and lattice distortion are analyzed by transmission electron microscope (TEM) and XRD reciprocal space mapping (RSM), respectively.

A. Magnetic and structural properties dependent on T_{ia}

The magnetic properties of $Fe_2Co_{0.5}Cr_{0.5}Si$ films annealed at T_{ia} are characterized along both MgO[100] and MgO[110] directions. All samples exhibit in-plane magnetization with easy axis along MgO[110], as shown in Fig. 1(a, b). The annealing temperature dependence of magnetic moments along the MgO[110] is shown in Fig. 1(c) and T_{ia} dependence of H_c and M_s is shown in Fig. 1(d). The small magnetization of the sample annealed at 350°C can be attributed to poor crystallization. As T_{ia} increases, $Fe_2Co_{0.5}Cr_{0.5}Si$ gradually possesses high M_s and square M-H loops. The maximum M_s observed at 450°C can be attributed to the improvement of chemical order. Besides, $Fe_2Co_{0.5}Cr_{0.5}Si$ annealed at 450°C shows a higher in-plane anisotropy energy, which can be observed from big difference of M-H loops along the MgO[110] and MgO[100] directions shown in Fig. 1(a, b). Besides, XRD θ-2θ scans and φ-scans in Fig. 1 of the supplementary material suggest that FCCS has promoted fourfold $L2_1$ phase after 450°C annealing process. Hence, T_{ia} of 450°C renders optimal magnetization and crystallization.

B. Magnetic and structural properties dependent on Co composition

Co doping composition dependence of magnetic, structural properties and surface morphology are studied using $Fe_2Cr_{1-x}Co_xSi$ (30nm). All samples are in situ annealed at 450°C. Figure 2 shows Co composition dependence of M-H loops measured by VSM at RT. The squareness ratio (SR) is defined as M_r/M_s. SR is nearly equal to 1 when Fe_2CrSi is doped with Co. This is probably because Co doping could suppress the Cr diffusion from the buffer layer, which results in a better crystallization. This means that there are more domains with easy axis along the MgO [110] direction. Therefore, Co doping can increase SR to 1. Moreover, the M_s increases with Co composition, which is consistent with the Slater-Pauling curve. The in-plane magnetic anisotropy energy density can be calculated by K_u=M_s*H_k/2, where H_k is the anisotropy field. The Co composition dependence of H_k and K_u

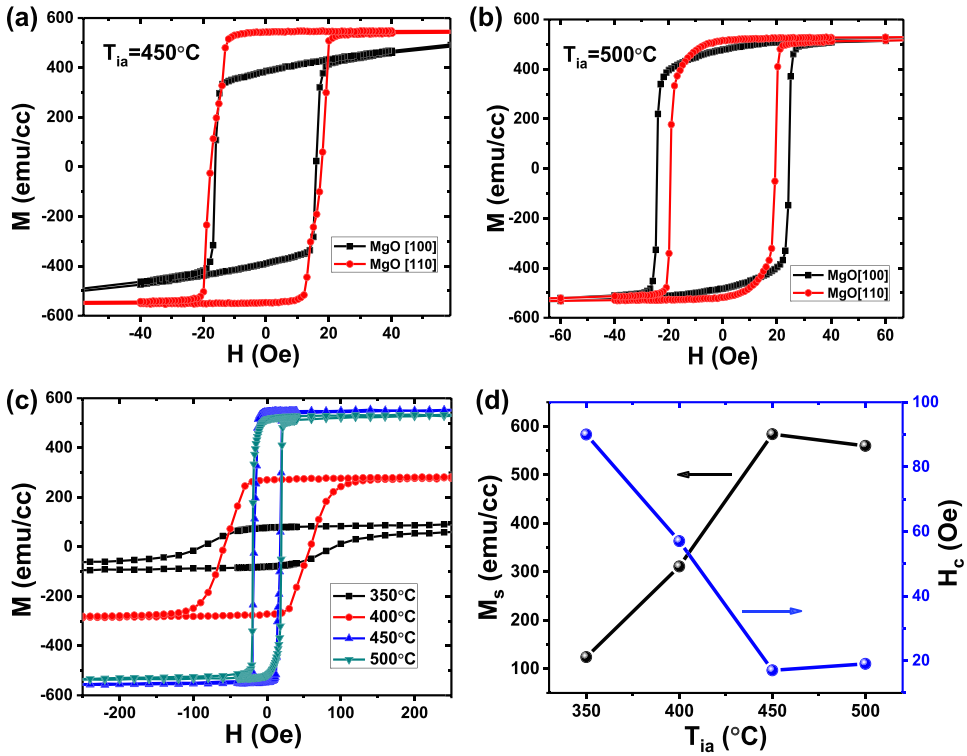

FIG. 1. (a, b) In-plane M-H loops of $Fe_2Cr_{0.5}Co_{0.5}Si$ along the MgO[100] and MgO[110] directions annealed at 450°C and 500°C, respectively, T_{ia} dependence of (c) M-H loops along the MgO[110] and (d) M_s and H_c of $Fe_2Co_{0.5}Cr_{0.5}Si$ films.

is shown in Fig. 3 of the supplementary material. As Co composition increases, both M_s and H_k contribute to an increasing K_u. The increase in M_s can be explained by Slater-Pauling curve and the increasing anisotropy field can be explained by the tetragonal lattice distortion. It has been proved that strain can greatly increase the magnetic anisotropy.[24] This is because tensile stress will dwindle the domains with magnetic moment perpendicular to the stress and render more magnetic moments parallel to the stress.[25] To further confirm this, we measured the lattice distortion dependent on Co doping in section C.

Phase and out-of-plane lattice parameter dependent on Co composition are studied in Fig. 2 of the supplementary material. The analysis shows vertical lattice reduces with Co doing. Appropriate Co doping helps FCCS promote $L2_1$ phase (25-50% Co doping) and higher Co doping will tune $L2_1$ phase gradually to $B2$ phase. Our result also suggests that within a regime of chemical disorder,

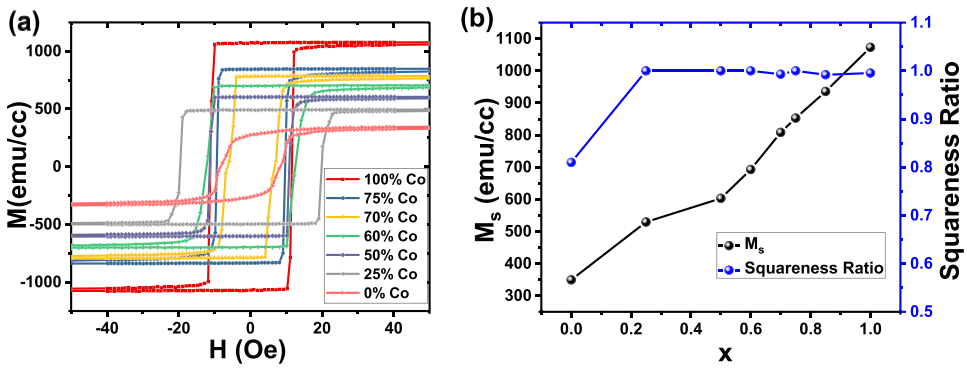

FIG. 2. (a) In-plane M-H loops and (b) M_s and Squareness ratio of $Fe_2Cr_{1-x}Co_xSi$ (30nm) films annealed at 450°C.

the magnetization is consistent with Slater-Pauling behaviour. AFM images demonstrate that high Co doping composition can reduce the roughness in Fig. 4 of the supplementary material.

C. Defects and lattice distortions dependent on Co composition

Buffer layer is proved to be crucial to enhance anisotropy of the ferromagnetic material (FM)/oxide interface.[26] The strains and defects induced in the substrates/buffer interface can affect magnetic properties of FM layer. Besides, the lattice mismatch is reported to be one of the reasons that PMA is generated.[27] Compared with Co-based Heusler, FCCS has the smaller lattice constant, which renders larger lattice mismatch at the Cr/FCCS interface. TEM and RSM measurements are carried out to further study the defects at the interfaces and lattice distortion of FCCS on Cr buffer layer. Our analysis of HRTEM images in Fig. 5 of the supplementary material suggests that FCCS has promoted a perfect lattice structure and smooth Cr/FCCS interface after 450°C annealing process.

The scanning TEM (STEM) is carried out to investigate the defects of $Fe_2Cr_{1-x}Co_xSi$ (x=0, 0.75, 1) layers as shown in Fig. 3. It can be clearly identified that Cr buffer has more defects than that of FCCS. The arrows indicate some defects in FCCS films either at the interface or through the whole layer. The defects induced at the interface can be attributed to lattice mismatch between the two layers. Note that Fe_2CrSi has the least defects compared with Fe_2CoSi. This is due to the smaller mismatch of Fe_2CoSi/Cr. $Fe_2Cr_{0.25}Co_{0.75}Si$ displays the highest defect density. This is probably because the Co and Fe atoms in quaternary Heusler alloys both prefer to occupy A, C sites in Wyckoff positions, which induces more defects. In summary, both higher Co composition and the doping effect contribute to a higher defect density.

Figure 4 shows the RSM images and the calculated lattice distortion when Co composition is 0, 0.5, 0.75, 1, respectively. The first set of maps are centered at (002) direction to examine whether there is difference in growth orientation between Cr and FCCS. The second set of maps cut through reciprocal space in the plane defined as $(\bar{1}\bar{1}2)$. This RSM shows the information about both in-plane (lateral) and out-of-plane (vertical) lattice parameters and hence the distortion. The Cr (002) and Cr $(\bar{1}\bar{1}2)$ peaks are separately chosen as the reference peaks due to the consistency of Cr buffer.

As shown in Fig. 4(a), L values of FCCS (004) peaks increase with the Co composition. This indicates that the out-of-plane lattice parameter decreases with Co doping. The tilt of $Fe_2Cr_{0.25}Co_{0.75}Si$ (004) peak is probably related to high density of defects and strains in $Fe_2Cr_{0.25}Co_{0.75}Si$. Accordingly, Fe_2CoSi (004) peak shows a slight tilt compared to other two samples. Besides, in the first RSM data set, there is no deviation from the h=0 axis for FCCS (004) peaks. This indicates that there is no growth orientation difference between Cr and FCCS lattices. Hence, the angle FCCS deviated from Cr $(\bar{1}\bar{1}2)$ show the degree of lattice distortion. In the RSM data second, all FCCS peaks

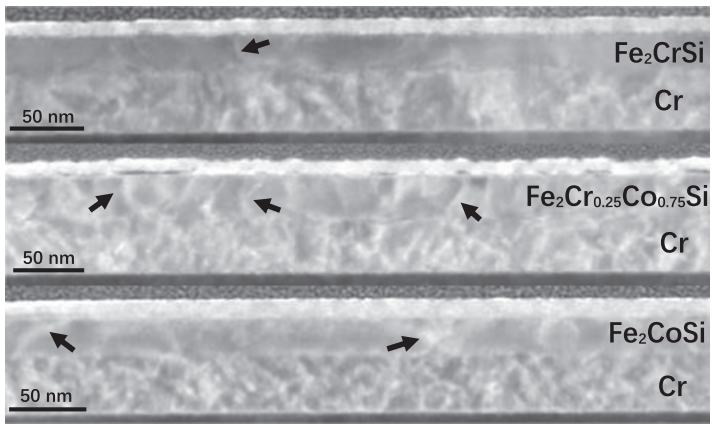

FIG. 3. Scanning TEM (STEM) images of the stack MgO(100)/Cr(35nm)/$Fe_2Cr_{1-x}Co_xSi$(30nm)/Ru(3nm). (x=0, 0.75, 1 for films from top to bottom, respectively).

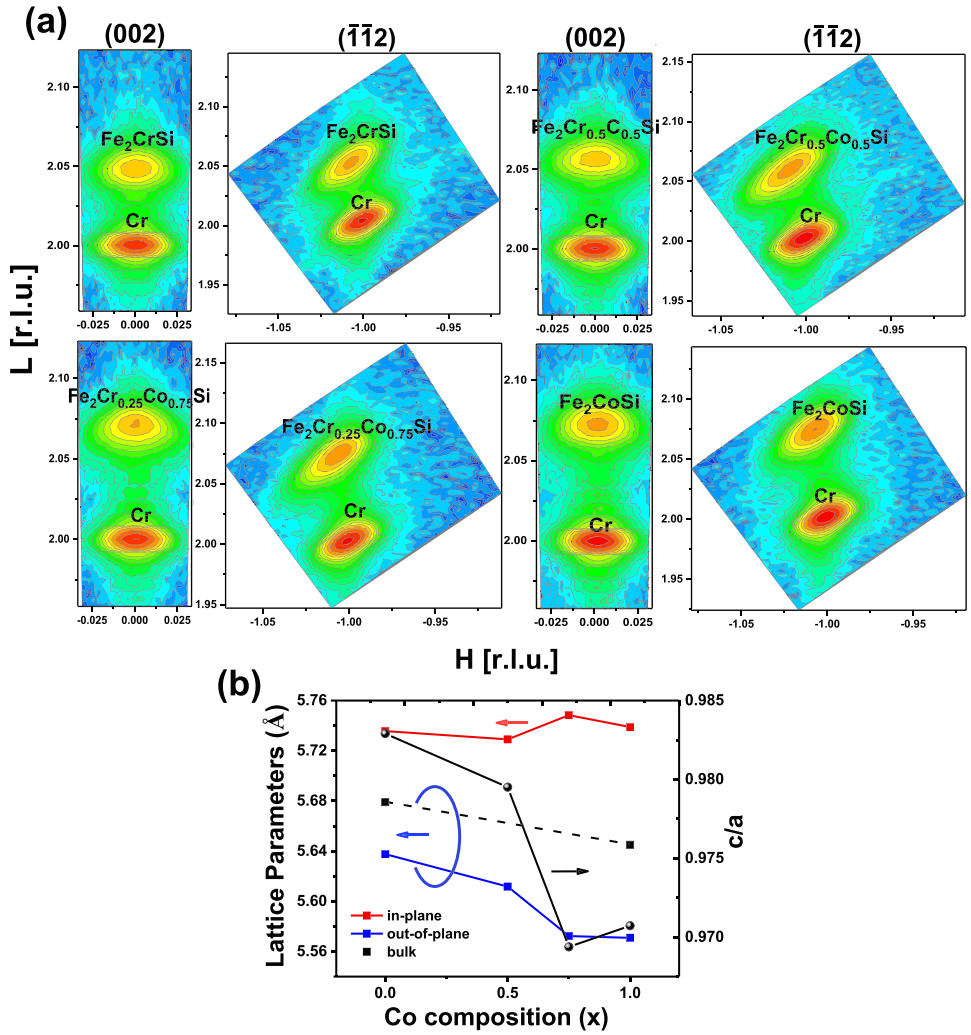

FIG. 4. (a) X-ray RSM separately centered at (002) direction and ($\bar{1}\bar{1}2$) direction of Cr and $Fe_2Cr_{1-x}Co_xSi$, x=0, 0.5, 0.75, 1, and (b) Co doping concentration dependence of the in-plane (red square), out-of-plane (blue square) lattice parameters and calculated lattice distortions (*c*/*a*) (black circle) from RSM of the film as well as the bulk lattice constant (dotted line) for comparison.[20]

are shifted from h=-1 axis. This indicates that there are lateral tensile strains among FCCS lattice. Here we assume that the Cr layer is fully relaxed based on our TEM results. According to Cr and FCCS peak positions in reciprocal space, lateral and vertical lattice parameters are calculated as shown in Fig. 4(b). The bulk lattice constants are measured using Fe_2CrSi and Fe_2CoSi ingots,[20] plotted as dotted line. The out-of-plane lattice parameter ($a^{\perp}$) decreases from 5.64Å to 5.57Å with Co composition increasing. However, all the in-plane parameters ($a_{//}$) are around 5.74Å, closer to 5.80Å, considering our experimental Cr lattice constant a_{Cr}=5.80Å/2. The in-plane lattice parameter of FCCS is larger than the bulk (dotted line) and the out-of-plane lattice parameter is smaller than the bulk. This indicates that all films are laterally stretched to match the Cr lattice during the epitaxial growth. The mismatch between buffer and Heusler is mainly relaxed by strain and the rest is relaxed by defects induced at the interface. The Co doping dependence of a_{bulk} plots lies in between $a^{\perp}$ and $a_{//}$ plots. This indicates that when in-plane lattice is stretched with Co doping, the out-of-plane lattice is compressed accordingly. This analysis suggests that the tetragonal distortion is caused by an elastic stress.

The lattice distortion defined as *c*/*a* is to assess the degree of the strains (black circles). On one hand, the lattice distortion increases linearly with Co doping composition. As discussed

in section B, the in-plane tensile stress strengthens the domains with in-plane magnetic moments. Therefore, the bigger distortions induced by higher Co doping composition would increase in-plane anisotropy energy. In Fig. 3 of the supplementary material, K_u of the $Fe_2Cr_{0.25}Co_{0.75}Si$ sample is out of the linear trend. This can also be explained by large lattice distortion of this sample.

The distortions show an increasing trend with Co doping which could explain the increase in the in-plane anisotropy energy density. On the other hand, defects formed in FCCS lattice also contribute to the lattice distortion. This can explain that $Fe_2Cr_{0.25}Co_{0.75}Si$ has the largest lattice distortion, followed by Fe_2CoSi, $Fe_2Cr_{0.5}Co_{0.5}Si$ and Fe_2CrSi. These distortions increase the anisotropy energy, however, don't change important magnetic properties like easy axis of magnetization or the coercivity.[16]

III. CONCLUSION

In this work, we investigated the effect of T_{ia} for $Fe_2Cr_{0.5}Co_{0.5}Si$ and determined the optimal annealing temperature. The effects of Co doping on magnetic properties, surface morphology, defects and lattice distortions are investigated. We found that the Co doping can increase the in-plane saturate magnetization and in-plane anisotropy energy density linearly. Additionally, the Co doping increases squareness ratio to 1 and reduces the surface roughness. Doping effect and lattice mismatch in Heusler alloys both contribute to the defects in FCCS leading to an increase in lattice distortion. The FCCS lattice tetragonal distortion increases with Co composition, which accounts for increasing in-plane anisotropy energy with Co doping.

SUPPLEMENTARY MATERIAL

See supplementary material for the (a) T_{ia} dependence of structural properties for $Fe_2Cr_{0.5}Co_{0.5}Si$ studied by XRD, (b) Co doping composition dependence of structural properties for $Fe_2Cr_{1-x}Co_xSi$ annealed at 450°C analyzed by XRD, (c) Anisotropy energy density, (d) Surface morphology dependent on Co doping composition demonstrated by AFM and (e) HRTEM of the interfaces for MgO sub/Cr and Cr/Fe_2CrSi.

ACKNOWLEDGMENTS

This work was supported by National Research Foundation, under Grant No. NRF-CRP12-2013-01. The authors would like to acknowledge the Singapore Synchrotron Light Source (SSLS) for providing the facility necessary for conducting the research.

[1] S. Trudel, O. Gaier, J. Hamrle, and B. Hillebrands, Journal of Physics D: Applied Physics **43**(19), 193001 (2010).
[2] Y. Miura, K. Nagao, and M. Shirai, Physical Review B **69**(14), 144413 (2004).
[3] I. Galanakis, P. Dederichs, and N. Papanikolaou, Physical Review B **66**(17), 174429 (2002).
[4] S. Wurmehl, G. H. Fecher, H. C. Kandpal, V. Ksenofontov, C. Felser, H.-J. Lin, and J. Morais, Physical Review B **72**(18), 184434 (2005).
[5] T. Kubota, S. Tsunegi, M. Oogane, S. Mizukami, T. Miyazaki, H. Naganuma, and Y. Ando, Applied Physics Letters **94**(12), 122504 (2009).
[6] H. Sukegawa, J. P. Hadorn, Z. Wen, T. Ohkubo, S. Mitani, and K. Hono, Applied Physics Letters **110**(11), 112403 (2017).
[7] Z. Wen, J. Kim, H. Sukegawa, M. Hayashi, and S. Mitani, AIP Advances **6**(5), 056307 (2016).
[8] Z. Wen, H. Sukegawa, S. Kasai, M. Hayashi, S. Mitani, and K. Inomata, Applied Physics Express **5**(6), 063003 (2012).
[9] L. M. Loong, J. H. Kwon, P. Deorani, C. N. Tung Yu, A. Hirohata, and H. Yang, Applied Physics Letters **104**(23), 232409 (2014).
[10] C. Sterwerf, S. Paul, B. Khodadadi, M. Meinert, J.-M. Schmalhorst, M. Buchmeier, C. K. Mewes, T. Mewes, and G. Reiss, Journal of Applied Physics **120**(8), 083904 (2016).
[11] S. He, Y. Liu, Y. Zheng, Q. Qin, Z. Wen, Q. Wu, Y. Yang, Y. Wang, Y. Feng, and K. L. Teo, Physical Review Materials **1**(6), 064401 (2017).
[12] A. Niesen, J. Ludwig, M. Glas, R. Silber, J.-M. Schmalhorst, E. Arenholz, and G. Reiss, Journal of Applied Physics **121**(22), 223902 (2017).
[13] Z. Wen, H. Sukegawa, T. Furubayashi, J. Koo, K. Inomata, S. Mitani, J. P. Hadorn, T. Ohkubo, and K. Hono, Advanced Materials **26**(37), 6483–6490 (2014).
[14] Y. Du, G. Z. Xu, E. K. Liu, G. J. Li, H. G. Zhang, S. Y. Yu, W. H. Wang, and G. H. Wu, Journal of Magnetism and Magnetic Materials **335**, 101–104 (2013).

[15] M. Ramudu, S. Inamdar, J. Arout Chelvane, M. Manivel Raja, and S. V. Kamat, Journal of Physics D: Applied Physics **49**(5), 055001 (2016).
[16] D. Sander, Reports on Progress in Physics **62**(5), 809 (1999).
[17] R. Skomski and J. Coey, Physical Review B **48**(21), 15812 (1993).
[18] M. Gabor, T. Petrisor, Jr., C. Tiusan, M. Hehn, and T. Petrisor, Physical Review B **84**(13), 134413 (2011).
[19] T. Kubota, Y. Ina, Z. Wen, H. Narisawa, and K. Takanashi, Physical Review Materials **1**(4) (2017).
[20] H. Luo, Z. Zhu, L. Ma, S. Xu, H. Liu, J. Qu, Y. Li, and G. Wu, Journal of Physics D: Applied Physics **40**(22), 7121–7127 (2007).
[21] Y.-P. Wang, S.-T. Lim, G.-C. Han, and K.-L. Teo, Journal of Applied Physics **118**(23), 233906 (2015).
[22] Y.-P. Wang, G.-C. Han, H. Lu, J. Qiu, Q.-J. Yap, and K.-L. Teo, Journal of Applied Physics **115**(17), 17C709 (2014).
[23] J. Du, S. Gnanarajan, and A. Bendavid, Superconductor Science and Technology **18**(8), 1035–1041 (2005).
[24] C. Yu, W. Wang, J. Chen, G. Wu, F. Yang, N. Tang, S. Qi, W. Zhan, Z. Wang, and Y. Zheng, Journal of Applied Physics **87**(9), 6292–6294 (2000).
[25] B. D. Cullity and C. D. Graham, *Introduction to magnetic materials*. (John Wiley & Sons, 2011).
[26] A. Davydenko, A. Kozlov, A. Ognev, M. Stebliy, A. Samardak, K. Ermakov, A. Kolesnikov, and L. Chebotkevich, Physical Review B **95**(6), 064430 (2017).
[27] M. Sakamaki, K. Amemiya, M. O. Liedke, J. Fassbender, P. Mazalski, I. Sveklo, and A. Maziewski, Physical Review B **86**(2) (2012).